PUBLICATIONS OF THE ASTRONOMICAL SOCIETY OF THE PACIFIC
93:5-19, February 1981

PUBLICATIONS OF THE
ASTRONOMICAL SOCIETY OF THE PACIFIC

Vol. 93 February 1981 No. 551

CLASSIFICATION PARAMETERS FOR THE EMISSION-LINE SPECTRA OF EXTRAGALACTIC OBJECTS

J. A. BALDWIN AND M. M. PHILLIPS

Cerro Tololo Inter-American Observatory,* Casilla 603, La Serena, Chile

AND

ROBERTO TERLEVICH

Institute of Astronomy, Madingley Road, Cambridge, England CB3 0HA

Received 1980 August 21

An investigation is made of the merits of various emission-line intensity ratios for classifying the spectra of extragalactic objects. It is shown empirically that several combinations of easily-measured lines can be used to separate objects into one of four categories according to the principal excitation mechanism: normal H II regions, planetary nebulae, objects photoionized by a power-law continuum, and objects excited by shock-wave heating. A two-dimensional quantitative classification scheme is suggested.

Key words: H II region—Seyfert galaxies—quasars—spectral classification

I. Introduction

The number of extragalactic emission-line objects for which accurate line intensities are available has grown rapidly over the past several years. Various authors have placed these objects into a rather confusing array of categories (narrow-line radio galaxies, broad-line radio galaxies, active galaxies, Seyfert 1, Seyfert 2, QSO, N galaxies, etc.) using classification schemes which depend more on the selection criteria, morphology, or line widths than on the information contained in the relative intensities of the emission lines. This has tended to obscure the factor which links many of these objects together most strongly, but which clearly separates others. This factor is the *excitation mechanism* operating on the line-emitting gas. From detailed studies, it is known that the predominant excitation mechanism in extragalactic objects is almost always one of the following: (a) photoionization by O and B stars, (b) photoionization by a power-law continuum source, or (c) shock-wave heating. A fourth excitation class is the planetary nebulae, which are photoionized by stars that are in most cases very much hotter than normal galactic O stars.

The growing body of data on emission-line galaxies has made increasingly obvious the need for a quantitative classification system which will give a direct measure of the main excitation mechanism operating on the gas. Since the different types of objects described above have characteristically different spectra, a classification system based on the relative strengths of emission lines would seem to offer a good chance of clearly distinguishing between the four possibilities. There is a long history of classifying planetary nebulae on the basis of the relative intensities of their emission lines (cf. Aller and Liller 1968). It is also well known that the emission-line spectra of galactic H II regions can be usefully classified according to intensity ratios such as $I([\mathrm{O\ III}]\ \lambda5007)/I(\mathrm{H}\beta)$ or $I([\mathrm{O\ II}]\ \lambda3727)/I([\mathrm{O\ III}]\ \lambda5007)$ (Searle 1971; Smith 1975; Alloin, Bergeron, and Pelat 1978), with the range in these parameters being provided mostly by the spread in heavy-element abundances among the different objects. Unfortunately, power-law photoionization or shock-wave heating are not easily distinguished in these one-parameter classification schemes. These types of objects are instead recognized by the presence of lines indicating simultaneously high ionization and low ionization. Such lines are frequently used as an excitation parameter in a very qualitative way, and less often (cf. Heckman 1980) as a quantitative discriminant.

In this paper we use the best available data to explore the usefulness of a number of possible parameters for setting up a more comprehensive classification system. For maximum utility, such a classification scheme should be

*Cerro Tololo Inter-American Observatory is supported by the National Science Foundation under contract No. AST 78-27879.

based on the most easily measured lines. Because the details of line widths, the presence of underlying stellar spectra, instrumental limitations, and other factors can strongly affect which lines are accurately measurable in a particular spectrum, it is desirable to be able to derive an object's classification from a variety of different sets of line strengths. We therefore attempt to tie the best of the classification parameters together into a single two-dimensional system which will carry with reasonable precision a reasonable amount of information about the conditions in the ionized gas. We confine our attention to emission-line regions which have strong forbidden lines. We hope that the resulting classification system, although only a modest extension of the existing practice in the field, will allow better intercomparison of the different types of emission-line objects, and the easier recognition of the most unusual of these objects.

II. The Data Base

Observational experience and published model calculations both suggest that the following lines might be useful for discriminating between different excitation mechanisms: [Ne v] λ3426, [O II] λ3727, He II λ4686, Hβ λ4861, [O III] λ5007, [O I] λ6300, Hα λ6563, and [N II] λ6584. Other potentially useful lines such as [Ne III] λ3869, [O III] λ4363, and Hγ λ4340 have been avoided because of measurement difficulties arising from blending with other emission and absorption lines.

A set of reasonably accurate data on the lines of interest was compiled from the literature, using as much as possible papers that contain large sets of internally consistent data. Table I lists the sources used. All line strengths are based on photoelectric measurements. In cases where the spectrum of an underlying stellar population could affect the measurements of the emission-line strengths, we made a particular effort to use only the higher-resolution (5 Å–10 Å) data obtained with the new generation of spectrometers.

We subdivided the objects in this data base into four groups according to their principal excitation mechanism. There is little ambiguity in classifying objects as either planetary nebulae or normal H II regions (from here on we will use the term "H II region" to mean gas ionized by normal galactic O and B stars).

For our prototype power-law photoionization cases we have lumped together Seyfert 2 galaxies and narrow-line radio galaxies, since Koski (1978) has shown that the relative emission-line intensities of these two groups of objects are indistinguishable. Koski also found that the "average" Seyfert 2 spectrum is approximately matched by a combination of the emission-line spectra of a typical planetary nebula and the Crab nebula, implying that the gas is photoionized by a relatively flat spectrum of photons. Comparison of this average spectrum to models of nebulae heated by power-law photoionization and by shock-heating again strongly points to photoionization by a flat spectrum. Although the best published models of this sort (Shields and Oke 1975; Boksenberg and Netzer 1977) fail badly at predicting the strength of the [O II] λ3727 emission line, recent models of planetary nebulae (Aller et al. 1980) suggest that the problem was due to an underestimate of the O^+ charge exchange cross section rather than to any misinterpretation of the principal excitation mechanism. As further examples of power-law photoionization, we also include in this group the best-measured narrow-line regions of Seyfert 1 galaxies.

The best examples of galaxies with shock-heated gas are NGC 1052 (Koski and Osterbrock 1976; Fosbury et al. 1978), M87 (Ford and Butcher 1979), and the so-called "LINERS" studied by Heckman (1980); all show the characteristic of a relatively large [O III] λ4363/λ5007 intensity ratio, combined with strong lines of [O I] and [O II] and relatively weak [O III] lines. We take as our shock-heated prototypes those objects from this group which have also been satisfactorily fitted to detailed shock-heating models.

Using these criteria, we assembled line strengths for 80 H II regions, 23 planetary nebulae, and 38 extragalactic objects presumed to be excited either by power-law radiation or shock-wave heating.

The general goal is to find combinations of intensity ratios which clearly separate, both from each other and from normal H II regions, those gas clouds excited by

TABLE I

References for Emission-Line Intensities

Reference	Type of Object(s)	Notes
Barker 1978	PN	1
Boksenberg and Netzer 1977	NLR-SY1	
Costero and Osterbrock 1977	NLRG	
Danziger 1974	H II	2
Davidson 1978	SNR	2
Dopita 1978	HH	
Dufour 1975	H II	2
Ford and Butcher 1979	SHG	
Fosbury et al. 1978	SHG	
Hawley 1978	H II	
Heckman 1980	SHG	
Koski 1978	SY2, NLRG	
Miller 1974	SNR	
Miller 1978	SNR	
Neugebauer et al. 1976	DXH II	
O'Connell et al. 1978	DXH II	
Osterbrock and Costero 1973	SNR	
Osterbrock and Dufour 1973	SNR	
Osterbrock and Koski 1976	NLR-SY1	
Osterbrock and Miller 1975	NLRG	
Peimbert and Costero 1969	H II	2
Peimbert and Torres-Peimbert 1971	PN	2
Peimbert and Torres-Peimbert 1974	H II	2
Peimbert et al. 1978	H II	2, 3
Searle and Sargent 1972	DXH II	
Smith 1975	H II	

Key. - H II = galactic H II region, DXH II detached extragalactic H II region, PN = planetary nebula, SNR = supernova remnant, HH = Herbig-Haro object, SHG = shock-heated galaxy, SY2 = Seyfert 2 galaxy, NLRG = narrow-line radio galaxy, NLR-SY1 = narrow-line region of a Seyfert 1 galaxy.

NOTES: - (1) VV3, M1-1, VV8, NGC 4361, M3-27, and HB 12 not included. (2) Only objects with measured [O I] λ6300 emission were included. (3) S 298 not included.

shock-heating and power-law photoionization. This first requires that the normal H II regions be confined to as tight a range as is possible in each parameter. For this purpose, reddening corrections were applied to all intensity ratios to give

$$(\lambda_1/\lambda_2) \equiv \log [I(\lambda_1)/I(\lambda_2)]_{\rm obs} + C_1 \log[I(\mathrm{H}\alpha)/I(\mathrm{H}\beta)]_{\rm obs} - C_2 \quad , \qquad (1)$$

where the reddening-corrected intensity ratio is written simply as (λ_1/λ_2). Table II lists values of C_1 and C_2 computed for the intensity ratios used in the following discussion. The Whitford (1958) reddening law (as parameterized by Miller and Mathews (1972)) was used, along with the assumption that the unreddened $H\alpha/H\beta$ ratio is 2.86 (as given by Brocklehurst (1971) for case B, $T_e = 10^4$, $N_e = 10^2$).

While the above reddening correction is justifiable for normal H II regions and planetaries, its application to extragalactic objects which are excited by power-law photoionization or shock-heating is uncertain at best. This is because in the latter case collisional excitation and self-absorption can affect the intrinsic Balmer decrement, and the properties and geometry of any possible dust are generally unknown. We have found that the excitation parameters discussed below can in fact discriminate between the different excitation mechanisms just as well with as without the reddening correction. The inclusion of the reddening correction, however, does serve to tighten up the relationship found for the normal H II regions, and can therefore facilitate the recognition of intermediate cases which might otherwise be lost in the increased scatter.

TABLE II

Reddening Coefficients

Intensity Ratio	C_1	C_2
(3426/3727)	0.26	0.12
(3426/5007)	1.24	0.56
(3727/5007)	0.98	0.45
(4686/4861)	0.14	0.07
(5007/4861)	-0.11	-0.05
(6300/5007)	-0.77	-0.35
(6300/6563)	0.12	0.05
(6584/5007)	-0.90	-0.40
(6584/6563)	-0.01	0.00

III. A Search for Useful Intensity Ratios

We have been unable to find any single intensity ratio which clearly separates all of the possible types of excitation. This indicates the need of a classification system based on at least two intensity ratios. Of the ratios which can be formed from the strongest lines, (λ3727/λ5007) gives the best-defined sequence leading from low-excitation H II regions through high-excitation H II regions and then on to the planetary nebulae. We have therefore tended to use this as one of the two excitation parameters, in spite of the rather large wavelength separation of the lines involved.

In forming other potentially useful intensity ratios, we have allowed ourselves to be guided by practical restrictions such as avoiding pairs of weak lines and choosing lines as close to each other in wavelength as possible (in order to minimize any error arising from the reddening correction). Also, classification schemes involving forbidden lines of different elements are more abundance-sensitive than those involving only one element plus the Balmer lines, and are therefore given lower weight.

These considerations led us to study a series of diagrams on which (λ3727/λ5007) is plotted against the following intensity ratios: (λ5007/λ4861), (λ6584/λ6563), (λ6300/λ6563), (λ4686/λ4861), (λ3426/λ3727), (λ3426/λ5007), and (λ6584/λ5007). The only other diagram to be considered was (λ6584/λ6563) vs. (λ5007/λ4861).

The (λ3727/λ5007) vs. (λ5007/λ4861) plot demonstrates the general utility of many of these diagrams. Just the H II regions and planetary nebulae are shown in Figure 1. There is a tightly defined relationship, such that objects lying more than about 0.5 in the logarithm away from this relationship would immediately be suspected of falling in a different category. The detached extragalactic H II regions, which are very metal-poor (Sargent and Searle 1970), are plotted with separate symbols to indicate that abundance variations do not greatly affect the locus of H II region points on this diagram. Figure 2 shows the previous diagram with the addition of the objects excited by power-law photoionization and shock-heating. These new points are seen to fall systematically above the line described by the H II regions. In fact, there are four rather distinct zones correponding to the four common excitation mechanisms. Plotting the intensity ratios of a newly discovered object onto this diagram could be expected to give immediate insight into the principal excitation mechanism at work.

The (λ3727/λ5007) vs. (λ6584/λ6563) diagram is seen in Figure 3. Again there are four distinct areas corresponding to the four excitation mechanisms, although in this case the planetary nebulae do not fit neatly onto the

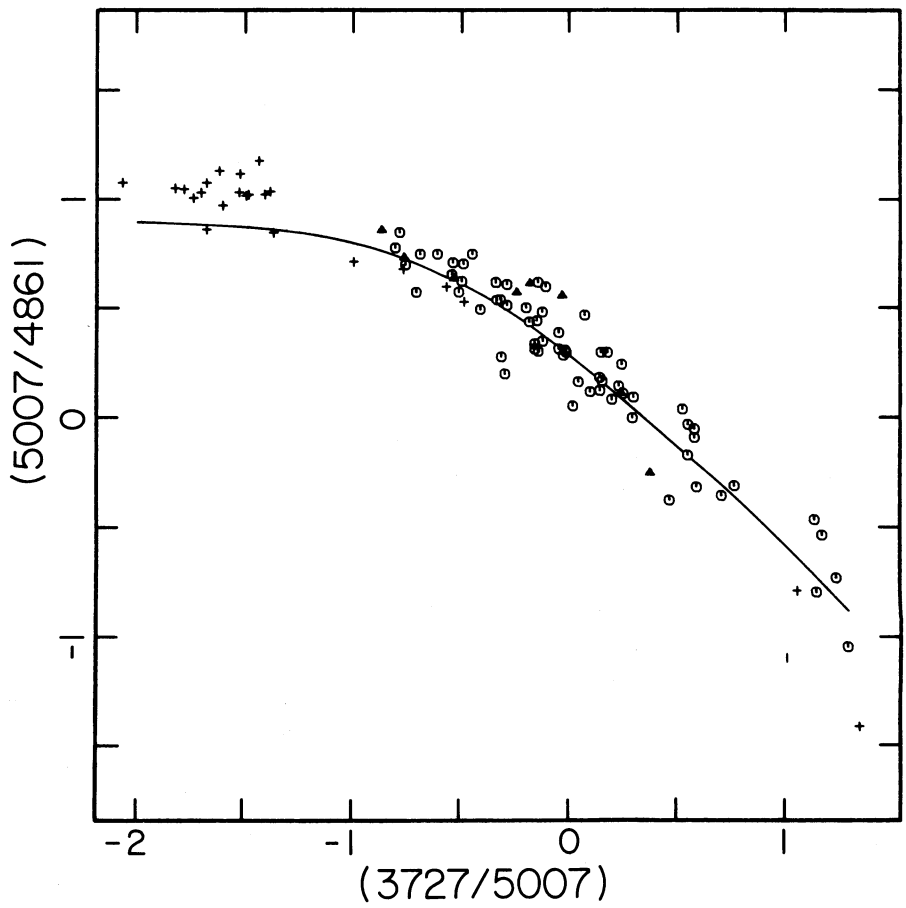

FIG. 1—The relationship between the (λ5007/λ4861) and (λ3727/λ5007) intensity ratios for H II regions and planetary nebulae. The intensity ratios are expressed in logarithms with reddening corrections applied as described in the text. Symbols: octagons = normal H II regions; triangles = detached extragalactic H II regions; "+" = planetary nebulae; vertical bar = upper limit on (λ5007/λ4861).

end of the sequence of H II regions. This diagram also offers considerable utility in identifying the principal excitation mechanism at work in a particular object.

The diagram for (λ3727/λ5007) vs. (λ6300/λ6563), shown in Figure 4, offers the cleanest separation that we have been able to find between the planetaries and H II regions on the one hand and power-law photoionization and shock-heating on the other. As has been realized for some time by workers in the field, the presence of [O I] λ6300 is a good indicator that one of the latter two excitation mechanisms is at work. From Figure 4, we can define the λ6300 line to be "present" if (λ6300/λ6563) $>$ -1.3. As was the case in the previous diagrams, the second dimension provided by (λ3727/λ5007) is needed to separate power-law photoionization from shock-heating, as well as the planetary nebulae from the H II regions.

In the (λ6584/λ6563) vs. (λ5007/λ4861) diagram of Figure 5, we have selected a new abscissa in order to use two intensity ratios in which the lines are close together in wavelength. Not only is this combination very insensitive to reddening, but it can be measured without the need for an accurate flux calibration, provided a linear detector is used. This diagram again shows four distinct regions, corresponding to the four excitation mechanisms, although in this case their orientation has been rotated somewhat. Both this diagram and that shown in Figure 3 have the drawback that we have used forbidden lines of both N and O, making the diagrams sensitive to the N/O abundance ratio.

The (λ3727/λ5007) vs. (λ6300/λ5007) diagram has previously been used to good advantage by Heckman (1980) to separate power-law photoionization from shock-heating. Figure 6 (which in fact includes much of Heckman's data) confirms his results, but shows that the H II regions are mixed in with the objects excited by other mechanisms more than was the case in some of the other diagrams. As both intensity ratios on this diagram involve lines with a fairly large wavelength spacing, we prefer to use (λ6300/λ6563) as an indicator of the relative strength of the [O I] line.

Similar problems arise with the (λ3727/λ5007) vs. (λ6583/λ5007) diagram, where the H II regions tend to overlap with the shock-heated objects and the intensity ratios involve lines at widely separated wavelengths and of several different elements. It has therefore not been pursued further.

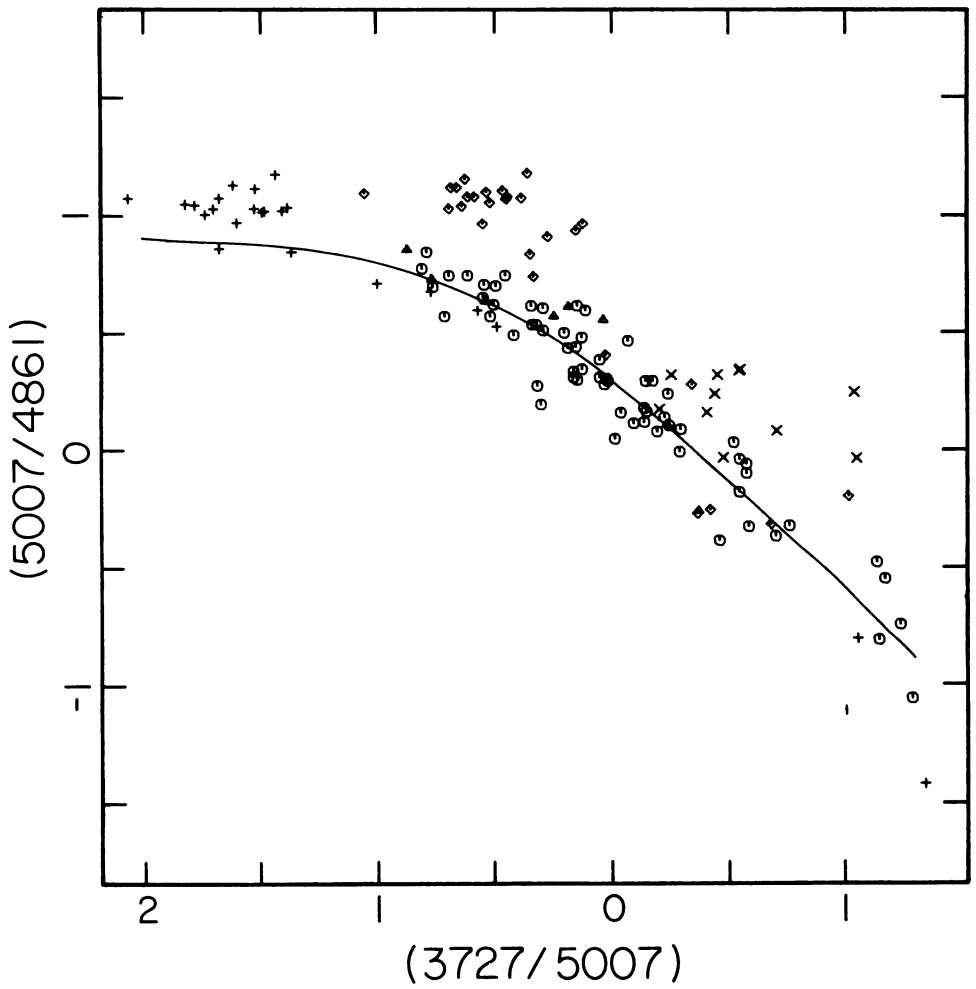

FIG. 2—The same as Figure 1, with the addition of objects photoionized by power laws (shown as diamonds), and shock-heated galaxies (shown as "x"s).

Surprisingly, the (λ3727/λ5007) vs. (λ4686/λ4861) diagram also fails to offer a clean separation between the different excitation mechanisms. The He II λ4686 line can be as strong in the higher-excitation H II regions as in objects excited by other means. Part of the problem here, though, may be the fact that there are measurements of λ4686 for only eight of the H II regions in our data set, and no upper limits are available for the others.

The final emission line which we had expected to be a good indicator of excitation mechanisms other than O and B stars is [Ne V] λ3426. Here again, the problem is that the line is *too* good at this task, to the extent that none of the H II regions in our sample had published measurements or limits for the line strength. Since it is one of the intrinsically weaker lines that we have used, and occurs at a short wavelength, there are no measurements of its strength in the shock-heated galaxies and only a few for the objects excited by power-law photoionization. From the sparse data which are available, it appears that (λ3426/λ5007) is probably a more sensitive discriminant than (λ3426/λ3727). Almost all of the (λ3426/λ5007) measurements available for our sample lie in the range −3.2 to 0.0. If we divide this range at the midpoint, (λ3426/λ5007) = −1.6, we find that the objects with larger (λ3426/λ5007) include all six of the available power-law photoionization points plus four planetary nebulae. Below this midpoint lie 13 planetaries, but no power-law photoionized objects. Lower yet, below (λ3426/λ5007) = −3.2, we find the one other planetary for which there is data, and presumably also all of the H II regions if upper limits were available. Our conclusion is that the (λ3727/λ5007) vs. (λ3426/λ5007) diagram has the potential of becoming another useful tool in the sort of two-dimensional classification system which we describe here, when and if the necessary calibrating data become available.

IV. Toward a Quantitative Classification Scheme

Having shown that there are a number of two-dimensional diagrams which can easily separate objects according to their principal excitation mechanism, we would next hope to construct a single classification scheme such

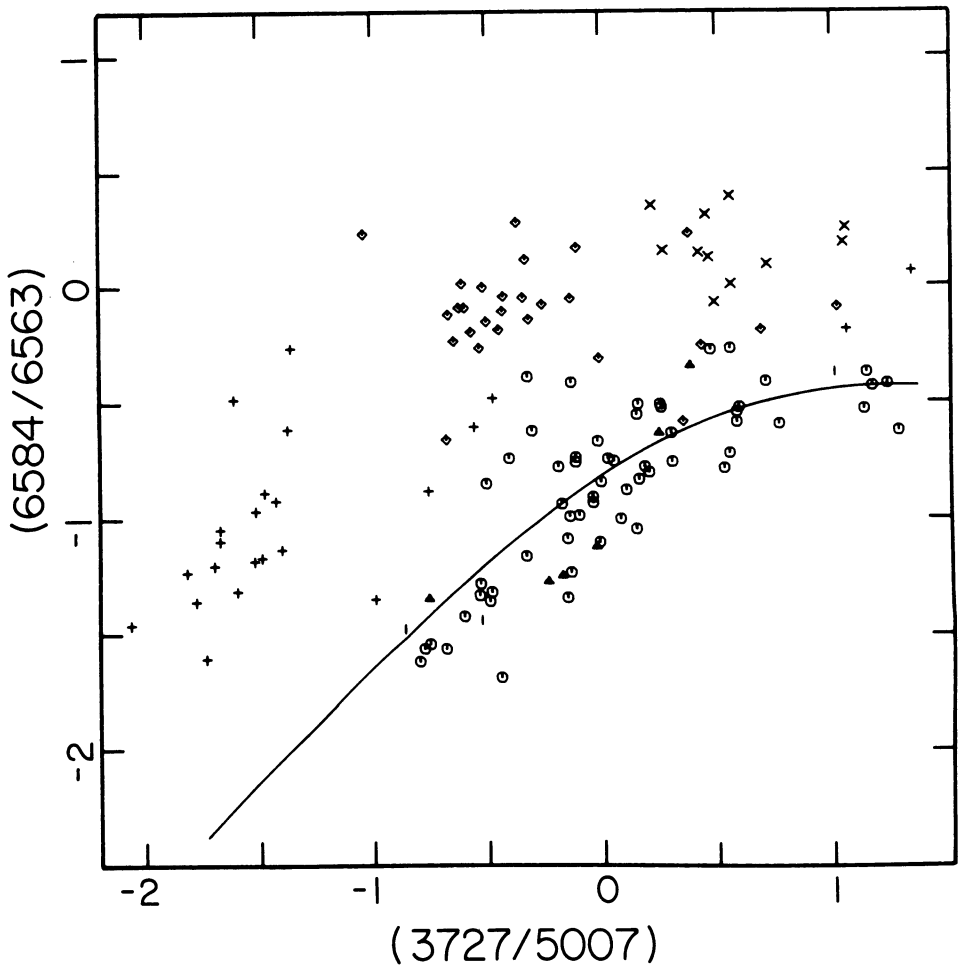

FIG. 3—The relationship between the (λ6584/λ6563) and (λ3727/λ5007) intensity ratios. The symbols have the same meanings as in Figures 1 and 2. Almost all of the upper limits (indicated by vertical bars) are for planetary nebulae.

that a given object will be given the same classification based on any of the intensity ratios used above. Although these ratios obviously reflect the important physical parameters in the emission-line regions, it is not clear how to use them to construct physically meaningful, orthogonal axes that would form a proper basis for the desired two-dimensional classification system. We therefore fall back to the simplest procedure, retaining (λ3727/λ5007) as one coordinate (in the diagrams where this intensity ratio is used, and then taking as the second parameter the vertical displacement in these diagrams from the locus of points representing the H II regions.

The first step in this procedure is to fit an analytic function through the points representing the H II regions. The predicted shape of this function can be found from a simplified model which follows Searle (1971) in supposing that each H II region is composed of just two ionization zones. The low-ionization zone is the He^0 region, and contains all of the O^+ and N^+ ions. It has a volume V_I. The high ionization, He^+ zone has volume V_{II} and contains all of the O^{++} ions. The Balmer lines originate from throughout the total volume, $V = V_I + V_{II}$. In this model, for fixed relative abundances and constant electron density N_e,

$$I(\mathrm{H}\beta) \propto I(\mathrm{H}\alpha\ \lambda6563) \propto N_e^2\, V \ , \quad (2)$$

$$I([\mathrm{O\ II}]\ \lambda3727) \propto I([\mathrm{N\ II}]\ \lambda6584) \propto N_e^2\, V_I \ , \quad (3)$$

and

$$I([\mathrm{O\ III}]\ \lambda5007) \propto N_e^2\, V_{II} \ . \quad (4)$$

These equations are readily solved, and the necessary constants evaluated by making least squares fits to the data, to obtain the curves shown in Figures 2, 3, and 5. The fits to the H II region data are seen to be quite adequate. The behavior of the planetary nebulae is *not* properly described by the model, but this is hardly surprising given that the planetaries have additional ionization zones and also tend to have different abundances.[1]

[1]In fact, several planetary nebulae which have been found by Torres-Peimbert and Peimbert (1977) to be extremely nitrogen-rich would extend into the area populated by power-law photoionization objects if their line intensities were plotted in Figures 1–6. Hence, it must be

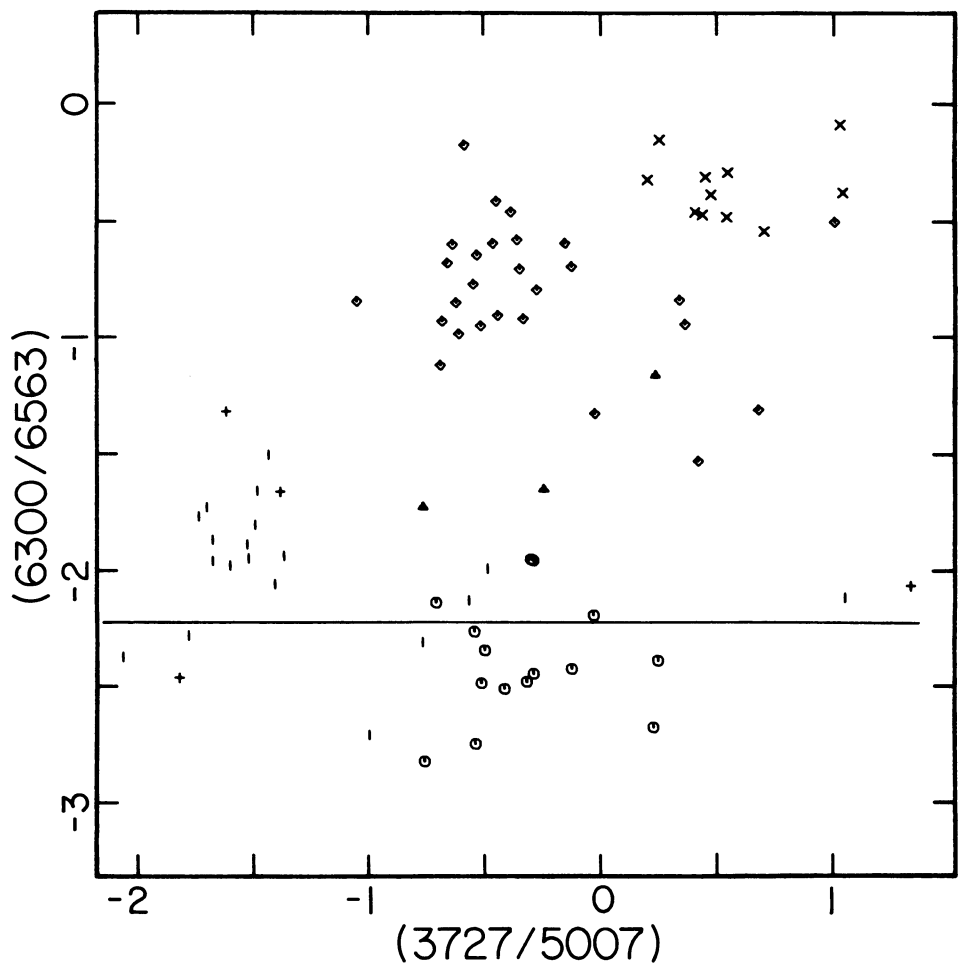

FIG. 4—The relationship between the (λ6300/λ6563) and (λ3727/λ5007) intensity ratios. The symbols have the same meanings as in Figures 1 and 2.

Next, the vertical displacement, which we will call the *excitation differences* $\Delta E(\lambda_1/\lambda_2)$, are computed by subtracting these fits from the observed points and applying appropriate normalization factors:

$$\Delta E\ (\lambda 5007/\lambda 4861) = (\lambda 5007/\lambda 4861) + \log(0.32 + x) - 0.44 \quad (5)$$

$$\Delta E\ (\lambda 6584/\lambda 6563) = 1/2[(\lambda 6584/\lambda 6563) - \log\ [x/(x + 1.93)] + 0.37] \quad , \quad (6)$$

where $x = I([\text{O II}]\ \lambda 3727)/I([\text{O III}]\ \lambda 5007)$ after the reddening correction. Our model does not predict the strength of [O I] λ6300 since there is no appropriate ionization zone. We have therefore just subtracted the mean (λ6300/λ6563) value for the H II regions and then normalized to obtain

$$\Delta E(\lambda 6300/\lambda 6563) = 1/5[(\lambda 6300/\lambda 6563) + 2.23] \quad . \quad (7)$$

The normalizing factors 1/2 and 1/5, which appear in equations (6) and (7), respectively, were estimated by taking the average, over all of the power-law photoionization objects and shock-heated galaxies, of the ratio of the relevant ΔE to $\Delta E(\lambda 5007/\lambda 4861)$. We caution the reader that there is a very large scatter in these ratios among the individual objects, as can be seen in the correlation diagrams presented in Figures 7a–c.

No attempt was made to put the points on the (λ6584/λ6563) vs. (λ5007/λ4861) diagram onto a ΔE scale. We did, however, fit our simple H II region model to the diagram, obtaining

$$(\lambda 5007/\lambda 4861) = \log\ [4.2 - 9.4I([\text{N II}]\ \lambda 6584)/I(\text{H}\alpha\ \lambda 6563)] \quad . \quad (8)$$

Comparison of this diagram to the others shows that points having constant (λ3727/λ5007) move away from the H II region line in the approximate direction indicated by the arrow in Figure 5.

Finally, we seek to combine the different ΔE indices

born in mind that peculiar abundances can never be entirely ruled out as an explanation for the unusual emission-line spectra of certain objects.

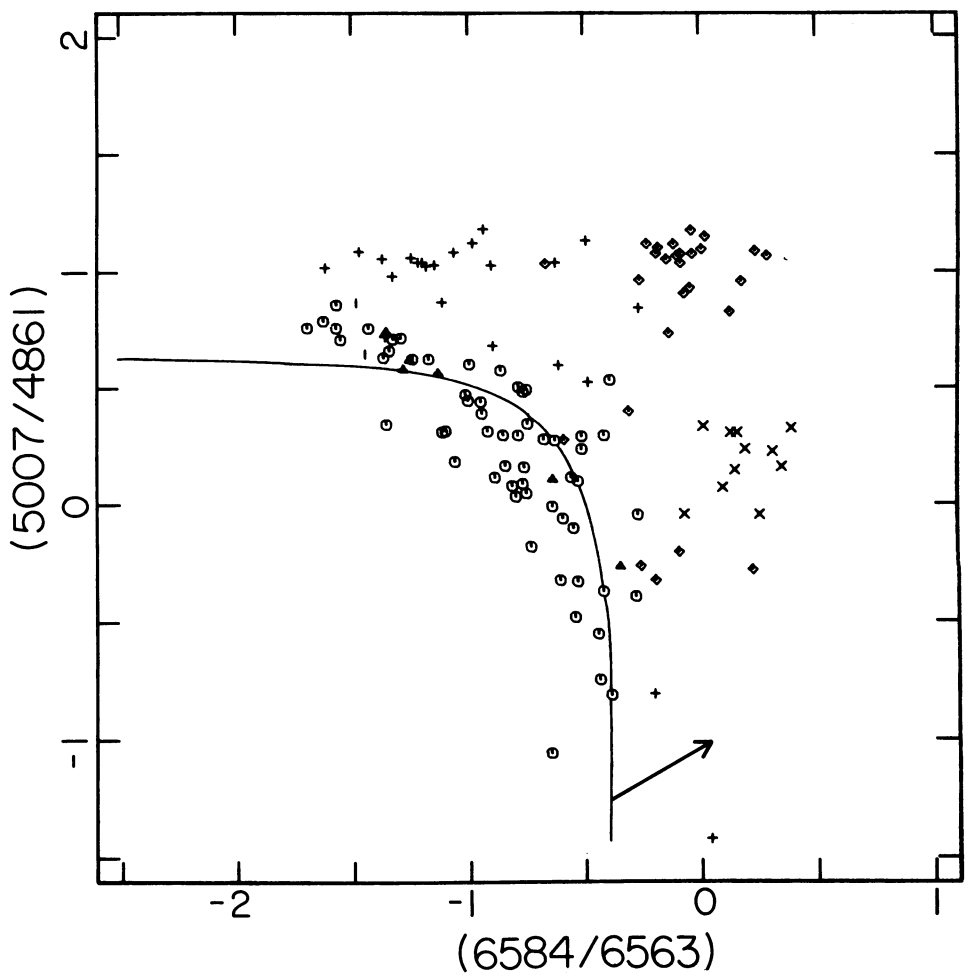

FIG. 5—The relationship between the (λ5007/λ4861) and (λ6584/λ6563) intensity ratios. The symbols have the same meanings as in Figures 1 and 2.

into a common system. If the same classification could be derived for an object on the basis of any of the intensity-ratio diagrams, the general properties of the spectra of different emission-line objects could be quickly and quantitatively compared even when the observations cover different regions of the spectrum. The desired strict correlation between the ΔE indices would of course be fortuitous, given that the various intensity ratios depend in different ways on the underlying physical variables. Figure 7 shows that the indices are in fact not well correlated. But there is still an advantage in averaging them together for each object, in order to bring into play as much data as are available and to help to define transition cases between different excitation mechanisms.

We define

$$\langle \Delta E \rangle = 1/3\,[\Delta E\,(\lambda 5007/\lambda 4861) + \Delta E\,(\lambda 6584/\lambda 6563) + \Delta E\,(\lambda 6300/\lambda 6563)]\ . \quad (9)$$

$\langle \Delta E \rangle$ is plotted against (λ3727/λ5007) in Figures 8 and 9. The H II regions scatter about $\langle \Delta E \rangle = 0$ with a Gaussian distribution having a standard deviation $\sigma = 0.064$. They all fall within the $\pm$ 3 σ limits shown in the figures. Most of the planetary nebulae lie inside a second region, as indicated in the figures, except that six are mixed in with the H II regions and could be either misclassified H II regions or planetaries having unusually cool stars. All of the shock-heated galaxies and most of the power-law photoionization objects fall clearly into their own distinct areas. There are in addition a few galaxies claimed to be photoionized by power-laws which scatter into other parts of the diagram, and which will be discussed in detail in section V. With the exception of the latter objects, the "power-law photoionization" zone on Figure 9 can be adequately described as $-1.3 <$ (λ3727/λ5007) < 0 and $\langle \Delta E \rangle > +0.19$, and the "shock-heated" zone as (λ3727/λ5007) ≥ 0 and $\langle \Delta E \rangle > +0.19$. The individual extragalactic objects used to define this classification system are listed in Table III.

V. Discussion

The primary goal of this work has been to find a variety of convenient graphs, using emission-line intensity ratios, which can segregate emission-line galaxies and QSOs according to their primary excitation mechanism.

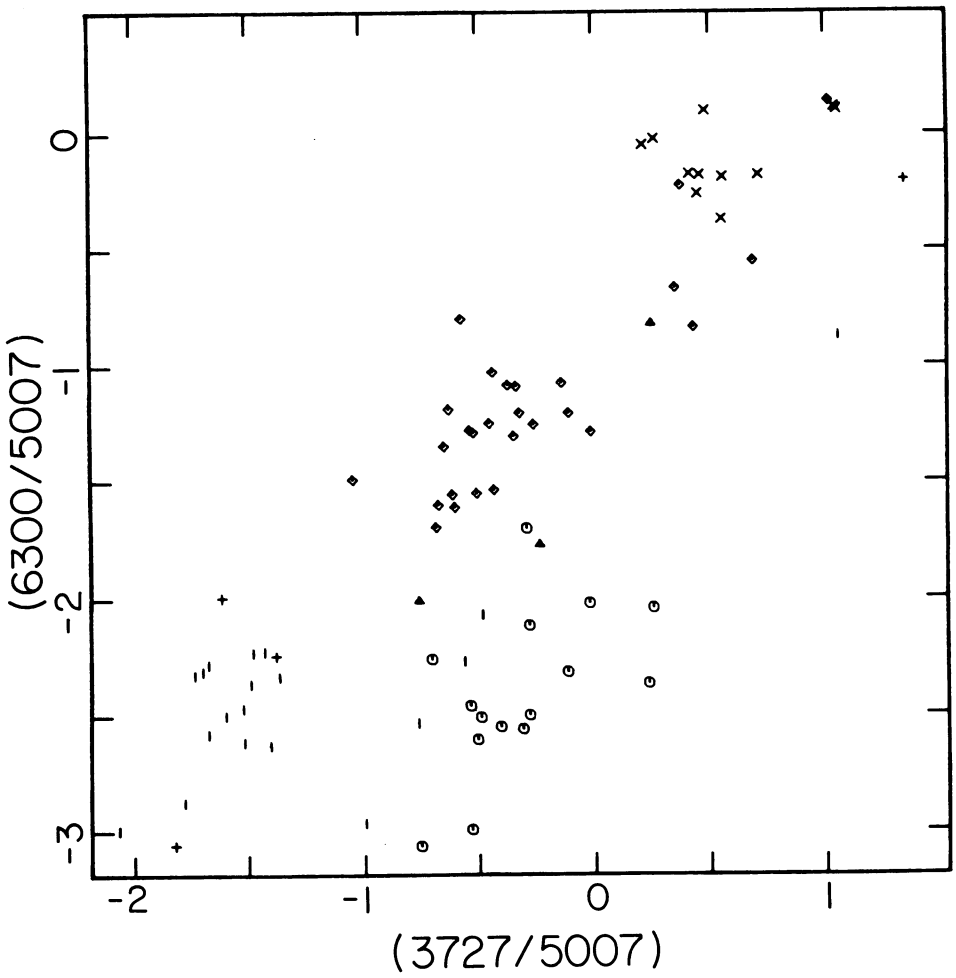

FIG. 6—The relationship between the (λ6300/λ5007) and (λ3727/λ5007) intensity ratios. The symbols have the same meanings as in Figures 1 and 2. Almost all of the upper limits (indicated by vertical bars) are for planetary nebulae.

This has proved to be quite easy. We can define a quantitative two-dimensional classification scheme which appears to offer some utility as a means for averaging together the different intensity ratios of a given object. It is not yet clear to us how this quantitative system can be anchored to parameters directly describing the physical conditions in each object.

The points of Figures 2–6 that represent shock heating all cluster together fairly tightly, but recent models (Dopita 1977; Shull and McKee 1979) predict that plausible variations in the gas density, the shock velocity, or the relative abundances could scatter the shock-heated objects over a much wider area on these diagrams. Including supernova remnants and Herbig-Haro objects does in fact produce a much greater scatter of points over the parts of the diagrams for which (λ3727/λ5007) $\geq$ 0. *Thus, part of the utility of our classification scheme must result from the rather small range in the parameters determining the spectra of extragalactic shock-heated objects.* However, only in the (λ5007/λ4861) vs. (λ6584/λ6563) diagram do any of the Galactic shock-heated objects (the supernova remnants) fall close to Koski's average Seyfert 2 galaxy. Therefore, it is probably safe to argue that an object in the "power-law photoionization zone" on these diagrams really is photoionized, provided that the case does not rest on just this one diagram.

Of greater concern is the possibility of confusing gas which is photoionized by very dilute power-law radiation with gas which is shock heated. Although the power-law ionization models have trouble correctly predicting the strengths of lines like [O II] λ3727, they still serve to indicate that the effect of an increasing dilution factor is to steadily increase (λ3727/λ5007) and decrease (λ5007/λ4861) while maintaining (λ6300/λ6563) at a high value (Baldwin et al. 1980). The question of whether this sort of emission-line region is found in nature can be investigated in two ways. The first is to look at the observed line strengths from gas which is known to be in the outermost parts of quasars and Seyfert galaxies (Wampler et al. 1975; Stockton 1976; Richstone and Oke 1977; Baldwin et al. 1980). These observations in all in-

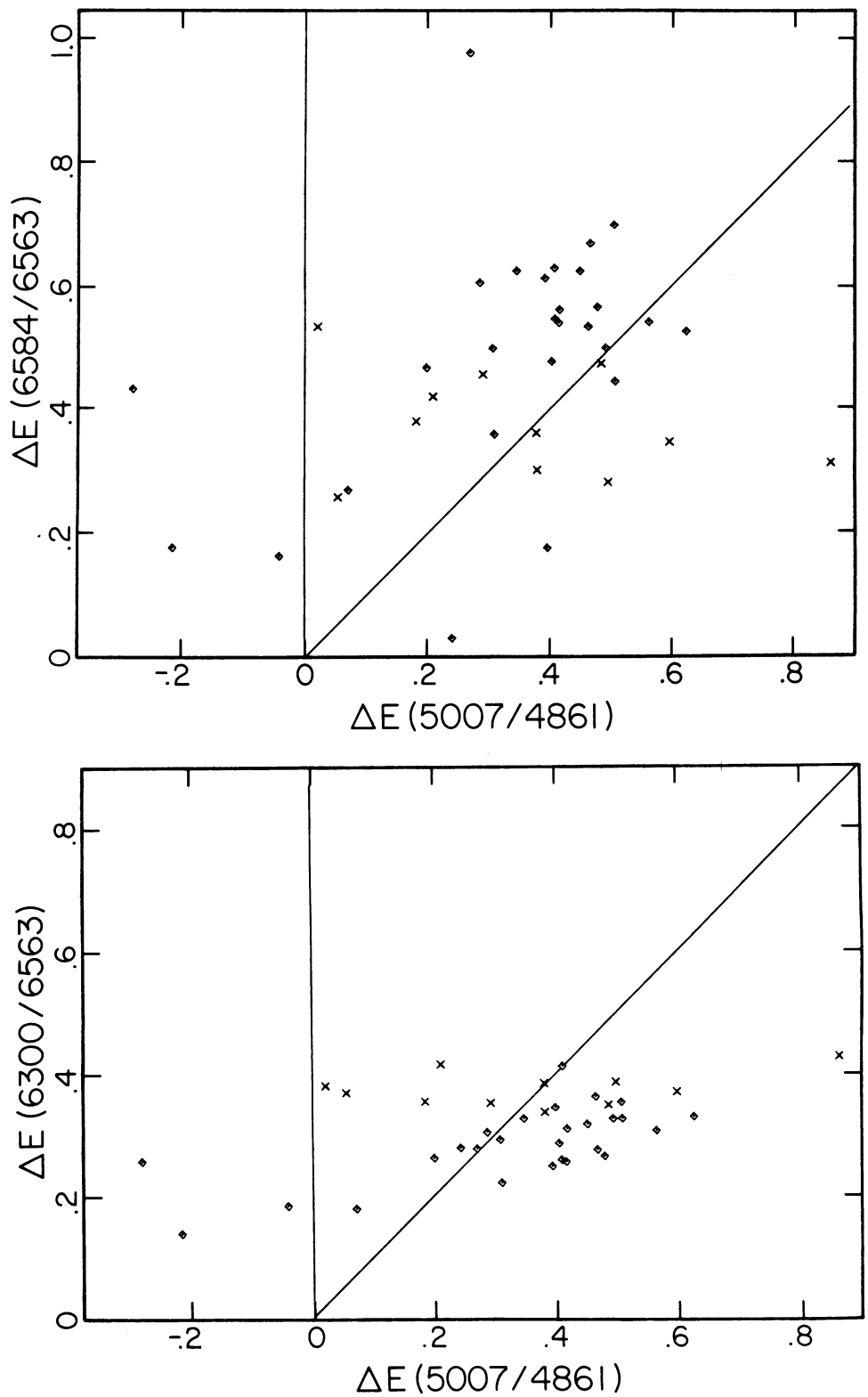

FIG. 7a–b—The poor correlation between the different ΔE indices is shown by the large scatter about the lines with slope 1. Symbols: same as in Figures 1 and 2.

stances lie in the power-law photoionization areas on our diagrams, so the dilution effect is *not* excessive even in cases where dilution is known to occur.

The second approach is to look at Seyfert 2 galaxies and narrow-line radio galaxies which lie outside the power-law photoionization limits of the diagrams. The

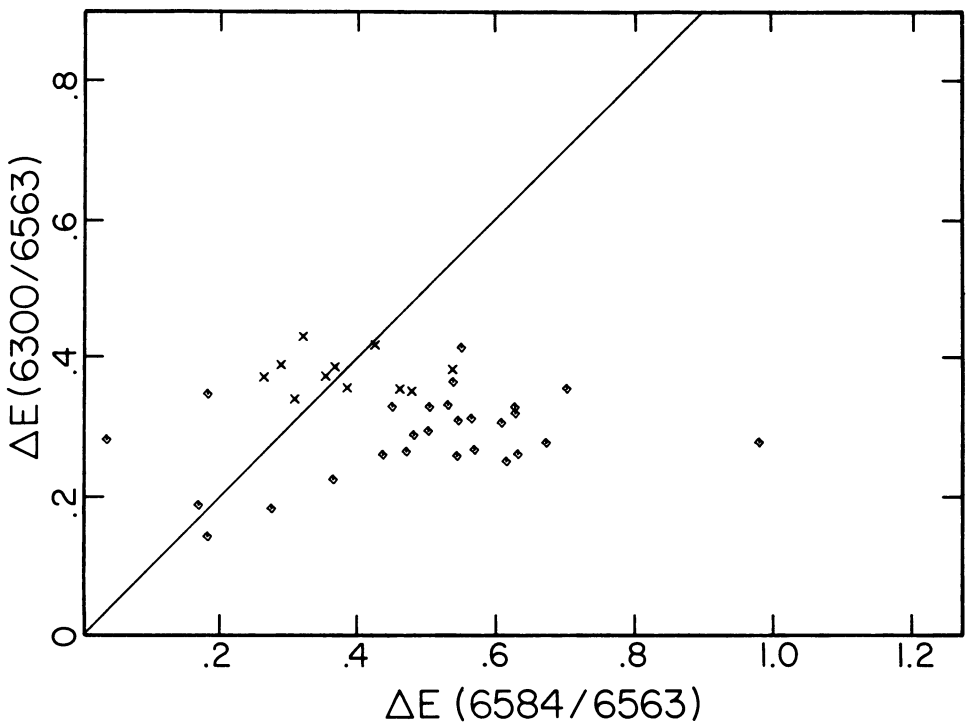

FIG. 7c—The poor correlation between the different ΔE indices is shown by the large scatter about the lines with slope 1. Symbols: same as in Figures 1 and 2.

four of these having the largest (λ3727/λ5007) indices are PKS 2322-12, Markarian 700, 3C 178, and NGC 6764, which are identified in Figure 9. Although Heckman (1980) has argued that the first two are predominantly shock heated, he was unable to fit models to the latter two galaxies. However, these have exceptionally blue continua showing Balmer absorption lines (Koski 1978; Costero and Osterbrock 1977), and their (λ6300/λ6563) indices are right at the borderline between the H II regions and shock-heated objects, suggesting that their emission-line spectra may be composites due to the action of more than one excitation mechanism. The two Seyfert 2 galaxies having the next highest (λ3727/λ5007) indices are Markarian 298 and Markarian 273. Heckman found that he could not fit them with shock-heating models either, and Koski has derived electron temperatures for the O^{++} zones which are far below those expected in the case of shock-heating. As their continuum energy distributions look just like those in the higher-excitation Seyfert 2's, it is possible that these two objects do represent very low-ionization cases of power-law photoionization. Alternatively, they could represent transition cases where photoionization by a nonthermal continuum *and* shock-heating are both important.

As examples of the application of this classification system, we have plotted in Figure 10 the $\langle \Delta E \rangle$ for several extragalactic objects of interest. Two of these, the radio galaxy Cygus A and the peculiar elliptical NGC 1052 have been extensively studied (Osterbrock and Miller 1975; Osterbrock and Koski 1976; Fosbury et al. 1978) and are prime examples of power-law photoionized and shock-excited emission regions, respectively. Also shown in Figure 10 are three galaxies whose nuclear regions Heckman concluded are H II regions photoionized by normal O and B stars, and six galaxies which he has singled out as power-law photoionized/shock-excited transition cases. Indeed, all of the former galaxies lie well within the boundaries defined by galactic H II regions. However, only four of the power-law photoionized/shock-excited transition cases (M 51 = NGC 5194, NGC 4258, Mkn 268, and 3C 452) would appear to meet that definition using the $\langle \Delta E \rangle$ values, while one (Mkn 273) is more consistent with shock-heated objects, and the other (Mkn 507) actually falls in the midst of the normal H II regions. The spectrum of this latter galaxy may well be contaminated by weak, broad Balmer-line emission similar to that found in Seyfert 1 galaxies and QSOs.[2] A similar explanation may account for the positions of the narrow-line "Fe II" galaxies Mkn 42 and 5C 3.100, which are also included in Figure 10. These galaxies are clearly undergoing some sort of unusual nuclear activity as evidenced by the presence of strong Fe II emission (Koski 1978), yet their $\langle \Delta E \rangle$ values are the same as those of normal H II regions. Alterna-

[2]The Seyfert 2 classification of Mkn 507 is due to Koski (1976). An uncertain classification as a type 1 Seyfert had been previously made by Klachikian and Weedman (1974).

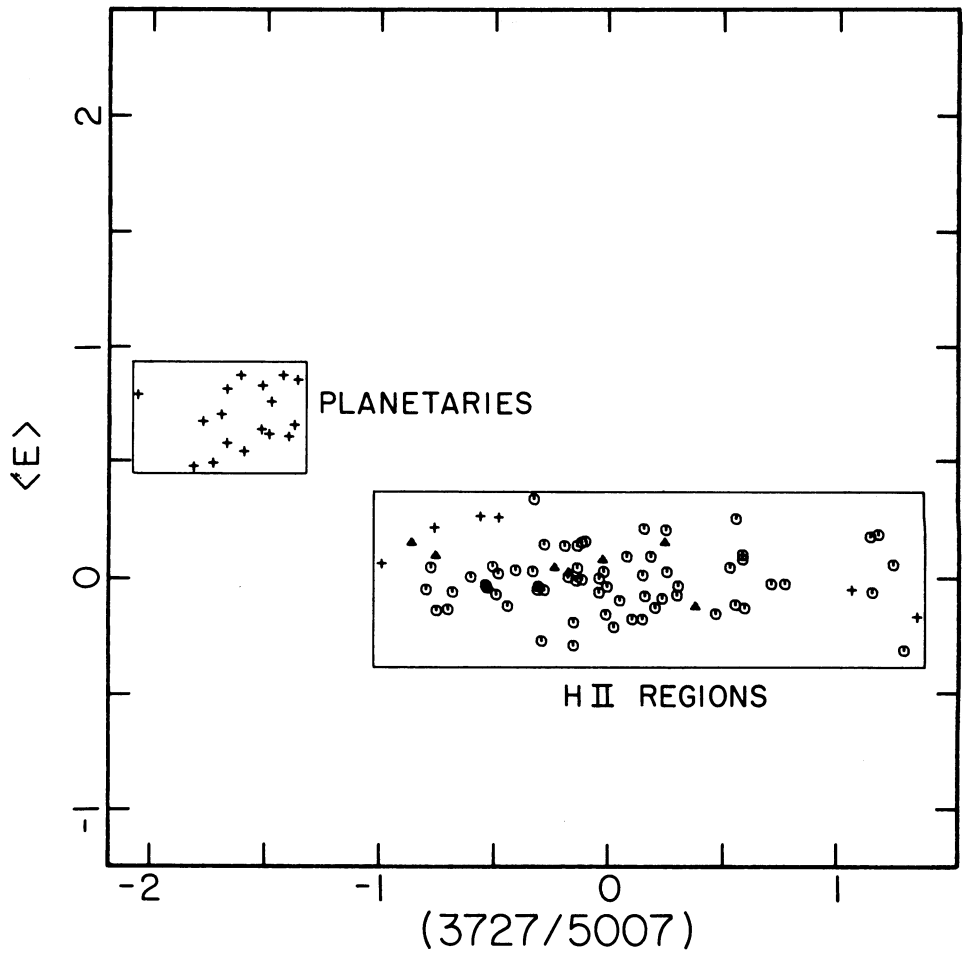

FIG. 8—The relationship between $\langle \Delta E \rangle$ (the average of the individual ΔE indices) and the (λ3727/λ5007) intensity ratio for planetaries and H II regions. Symbols: same as in Figure 1.

tively, the discrepant $\langle \Delta E \rangle$ of the Fe II galaxies and Mkn 507 could be due to the added presence of emission from normal H II regions. In such cases, high-resolution observations of the emission lines are needed to discern the exact nature of the nuclear activity.

A further intriguing example is 1400 + 162, which is generally classified as a BL Lacertae object but which has easily measurable [O II] λ3727 emission. From the figure published by Baldwin et al. (1977), we estimate (λ3727/λ5007) $\geq$ 0.2. This would suggest that the excitation is due to shock heating or hot stars rather than to photoionization by the nonthermal continuum, making perhaps even more confusing the interpretation of the weakness of the emission spectrum in this object. This is a more extreme example of the case of 3C 371, where enough emission lines have been observed (Miller 1975) to show that the spectrum is very similar to that of NGC 1052 and is therefore almost certainly shock heated, in spite of the presence of a strong power-law continuum.

VI. Summary

It has been shown that the emission-line spectra of most extragalactic objects are easily classified, using the relative intensities of the strongest lines, into groups corresponding to the predominant excitation mechanisms. These groups are: normal H II regions (photoionized by O and B stars), power-law photoionization, and shock-wave heating. For convenience, we have also carried a sample of planetary nebulae through our analysis, and these are easily separated from the rest.

A graphical approach to classifying objects into these four categories involves the intensity ratios of pairs of strong emission lines which measure various aspects of the excitation level in each object. We have found that the four groups can be effectively segregated using plots of (λ6584/λ6563) vs. (λ5007/λ4861), and of (λ3727/λ5007) against (λ5007/λ4861), (λ6584/λ6563), or (λ6300/λ6563).

In an effort to quantify this classification system, we have defined in equations (1), (5), (6), and (7) *excitation differences*, which we call ΔE. Although the values of ΔE derived from different line ratios for the same object are not very well correlated, it is still advantageous to average the different values together to obtain $\langle \Delta E \rangle$, as de-

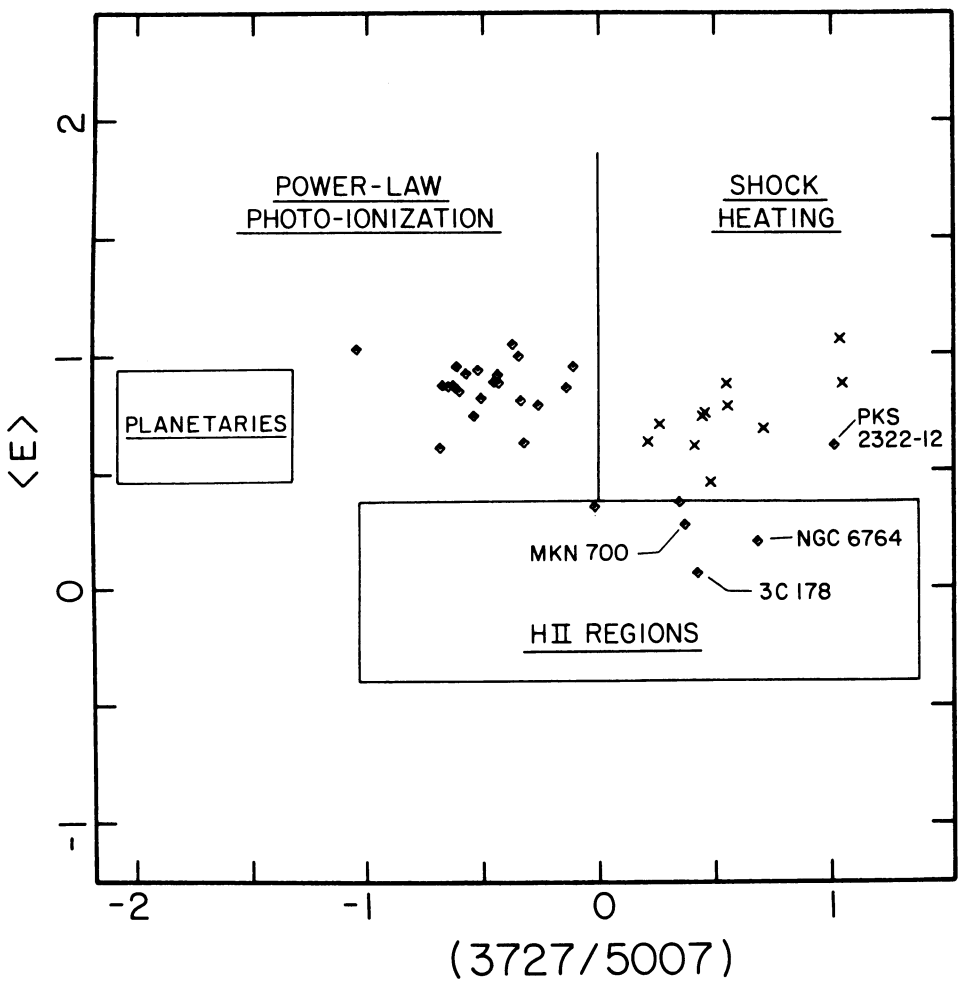

FIG. 9—The same as Figure 8, except showing objects photoionized by power laws (indicated by diamonds) and shock-heated galaxies ("+" symbols). A few individual galaxies discussed in the text are indicated by name.

fined in equation (9). A plot of $\langle \Delta E \rangle$ against (λ3727/λ5007) is then shown to be a useful tool for classifying emission-line spectra.

We wish to thank Dr. François Schweizer for helpful comments on the manuscript. R.T. gratefully acknowledges support from the Ludgren Fund of the University of Cambridge.

REFERENCES

Aller, L. H., and Liller, W. 1968, in *Nebulae and Interstellar Matter*, B. W. Middlehurst and L. H. Aller, eds. (Chicago: The University of Chicago Press), p. .
Aller, L. H., Keyes, C. D., Czyzak, S. J., and Shields, G. A. 1980 (preprint).
Alloin, D., Bergeron, J., and Pelat, D. 1978, *Astr. and Ap.* 70, 141.
Baldwin, J. A., Carswell, R. F., Wampler, E. J., Smith, H. E., Burbidge, E. M., and Boksenberg, A. 1980, *Ap. J.* 236, 388.
Baldwin, J. A., Wampler, E. J., Burbidge, E. M., O'Dell, S. L., Smith, H. E., Hazard, C., Nordsieck, K. H., Pooley, G., and Stein, W. A. 1977, *Ap. J.* 215, 408.
Barker, T. 1978, *Ap. J.* 219, 914.
Boksenberg, A., and Netzer, H. 1977, *Ap. J.* 212, 37.
Brocklehurst, M. 1971, *M.N.R.A.S.* 153, 471.
Costero, R., and Osterbrock, D. E. 1977, *Ap. J.* 211, 675.
Danziger, I. J. 1974, *Ap. J.* 193, 69.
Davidson, K. 1978, *Ap. J.* 220, 177.
Dopita, M. A. 1977, *Ap. J. Suppl.* 33, 437.
——— 1978, *Ap. J. Suppl.* 37, 117.
Dufour, R. J. 1975, *Ap. J.* 195, 315.
Ford, H. C., and Butcher, H. 1979, *Ap. J. Suppl.* 41, 147.
Fosbury, R. A. E., Mebold, U., Goss, W. M., and Dopita, M. A. 1978, *M.N.R.A.S.* 183, 549.
Hawley, S. A. 1978, *Ap. J.* 224, 417.
Heckman, T. M. 1980 (preprint).
Khachikian, E. Y., and Weedman, D. W. 1974, *Ap. J.* 192, 581.
Koski, A. T. 1976, Ph.D. Dissertation, University of California, Santa Cruz.
——— 1978, *Ap. J.* 223, 56.
Koski, A. T., and Osterbrock, D. E. 1976, *Ap. J.* (*Letters*) 203, L49.
Miller, J. S. 1974, *Ap. J.* 189, 239.
——— 1975, *Ap. J.* (*Letters*) 200, L55.
——— 1978, *Ap. J.* 220, 490.
Miller, J. S., and Mathews, W. G. 1972, *Ap. J.* 172, 593.
Neugebauer, G., Becklin, E. E., Oke, J. B., and Searle, L. 1976, *Ap. J.* 205, 29.
O'Connell, R. W., Thuan, T. X., and Goldstein, S. J. 1978, *Ap. J.* (*Let-*

TABLE III

Classifications of Extragalactic Emission-Line Objects

Name	(3727/5007)	< E >
Shock-Heated Galaxies:		
NGC 1052	.55	.39
NGC 2841	.41	.31
NGC 2911	.44	.37
NGC 3031	.45	.38
NGC 3998	.48	.23
NGC 4036	1.05	.44
NGC 4278	.71	.34
NGC 4486 (M87 nucleus)	.21	.31
NGC 4486 (M87 filaments)	.55	.44
NGC 5077	.26	.36
NGC 5371	1.04	.54
Objects Photoionized by Power Laws:		
Seyfert Galaxies:		
Mkn 1	-.63	.44
Mkn 3	-.53	.47
Mkn 34	-.51	.41
Mkn 78	-.44	.44
Mkn 176	-.62	.47
Mkn 198	-.33	.31
Mkn 270	-.15	.43
Mkn 298	.34	.19
Mkn 348	-.44	.46
Mkn 573	-.61	.42
Mkn 700	.37	.14
NGC 1068	-1.05	.51
NGC 6764	.68	.10
III Zw55	-.34	.40
Narrow-Line Radio Galaxies:		
3C 33	-.46	.44
3C 98	-.35	.50
3C 178	.42	.36
3C 184.1	-.69	.30
3C 192	-.27	.39
3C 327	-.68	.44
3C 433	-.12	.47
CYG A	-.38	.52
PKS 2322-12	1.01	.31
QSO/Seyfert 1 Narrow-Line Regions:		
Mkn 6	-.54	.37
Mkn 315	-.02	.18
NGC 3516	-.58	.46
NGC 4151	-.65	.43

ters) **226**, L11.
Osterbrock, D. E., and Costero, R. 1973, *Ap. J.* (*Letters*) **184**, L71.
Osterbrock, D. E., and Dufour, R. J. 1973, *Ap. J.* **185**, 441.
Osterbrock, D. E., and Koski, A. T. 1976, *M.N.R.A.S.* **176**, 61P.
Osterbrock, D. E., and Miller, J. S. 1975, *Ap. J.* **197**, 535.
Peimbert, M., and Costero, R. 1969, *Bol. Obs. Tonantzintla y Tacubaya* **5**, 3.
Peimbert, M., and Torres-Peimbert, S. 1971, *Bol. Obs. Tonantzintla y Tacubaya* **6**, 21.
Peimbert, M., Torres-Peimbert, S., and Rayo, J. F. 1978, *Ap. J.* **220**,
——— 1974, *Ap. J.* **193**, 327.
Peimbert, M., Torres-Peimbert, S., and Rayo, J. F. 1978, *Ap. J.* **220**, 516.
Richstone, D. O., and Oke, J. B. 1977, *Ap. J.* **213**, 8.
Sargent, W. L. W., and Searle, L. 1970, *Ap. J.* (*Letters*) **162**, L155.
Searle, L. 1971, *Ap. J.* **168**, 327.
Searle, L., and Sargent, W. L. W. 1972, *Ap. J.* **173**, 25.
Shields, G. A., and Oke, J. B. 1975, *Ap. J.* **197**, 5.
Shull, J. M., and McKee, C. F. 1979, *Ap. J.* **227**, 131.
Smith, 1975, .
Stockton, A. 1976, *Ap. J.* (*Letters*) **205**, L113.
Torres-Peimbert, S., and Peimbert, M. 1977, *Rev. Mex. de Astr. y Astrof.* **2**, 181.
Wampler, E. J., Robinson, L. B., Burbidge, E. M., and Baldwin, J. A. 1975, *Ap. J.* (*Letters*) **198**, L49.
Whitford, A. E. 1958, *A.J.* **63**, 201.

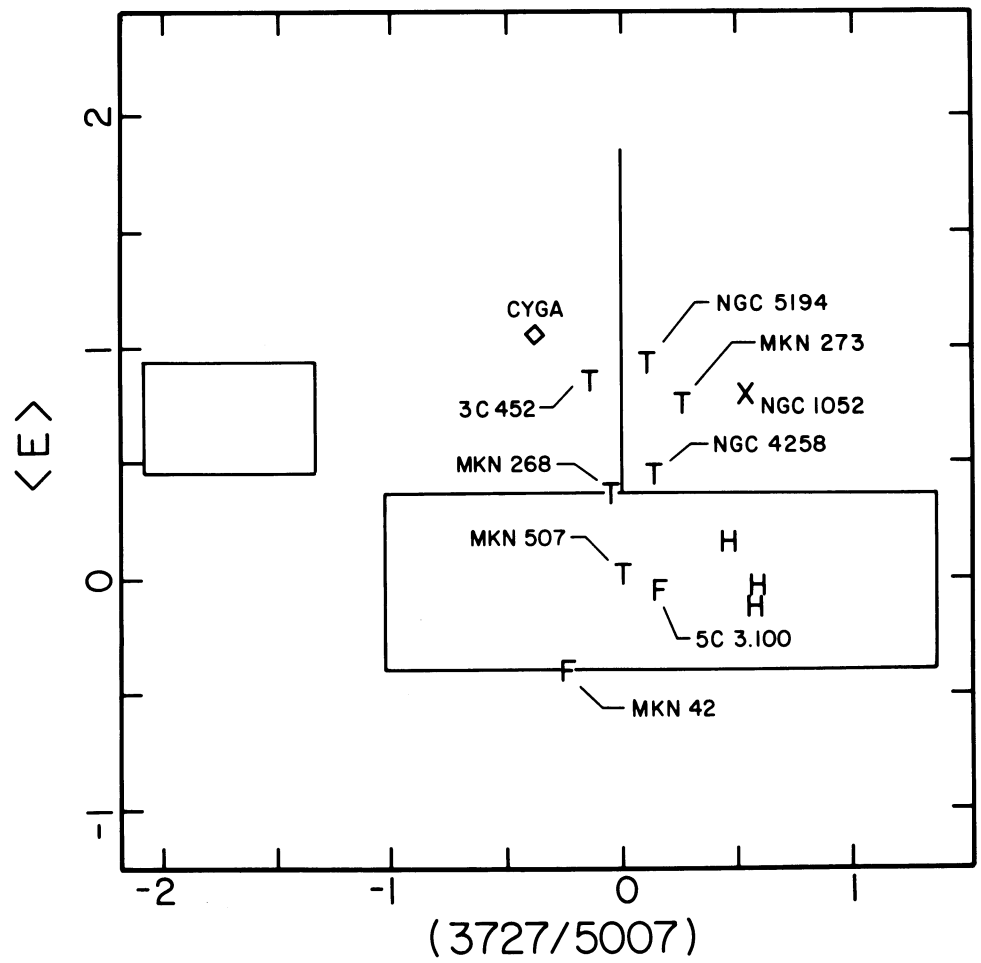

FIG. 10—The same as Figure 9, except showing galaxies which are not calibrators for our classification scheme. Symbols: "H" = Heckman "H II-region" galaxy; "T" = Heckman "transition" galaxy; "F" = narrow-lined Fe II galaxy. Cyg A and NGC 1052 are prototype examples of, respectively, power-law photoionization and shock heating.